nature communications

Article

https://doi.org/10.1038/s41467-025-61183-5

Dual origin of effective axion response

Received: 19 September 2024

Accepted: 15 June 2025

Published online: 01 July 2025

Check for updates

Timur Z. Seidov, Eduardo Barredo-Alamilla, Daniel A. Bobylev, Leon Shaposhnikov, Maxim Mazanov & Maxim A. Gorlach

Effective axion fields emerge in condensed matter and photonic systems with broken parity and time-reversal symmetries resulting in nonreciprocal optical phenomena. Here, we predict a distinct type of electromagnetic response which has the same symmetry properties as an axion one, manifests itself only at the boundaries of the material and features the same coupling to incident plane waves. However, the response to the external sources introduced inside is profoundly different, allowing one to distinguish the predicted dual axion field experimentally. We prove that the behavior of such materials is captured by electrodynamics with magnetic charge, put forward a specific metamaterial realizing this physics and suggest possible experiments to observe it. We anticipate that this response is general and occurs in a variety of photonic and condensed matter structures.

Effective description of condensed matter and photonic structures allows one to reduce their complex behavior to relatively simple theoretical models ignoring redundant degrees of freedom and introducing several key parameters. This approach features profound analogies with quantum field theory. For instance, the physics of relativistic Dirac fermions is reproduced in graphene, condensed matter and photonic systems described by the Dirac effective Hamiltonian[1–3]. Quantum Hall effect can be concisely described using the effective Chern-Simons Lagrangian[4,5], and the physics of topological insulators including quadrupole insulators is captured by the field-theoretical language[6,7].

Given their versatility, condensed matter and photonic structures can be a source of various effective theories, sometimes even without a known counterpart within the Standard Model. In this spirit, hypothetical axions[8,9] that evaded their experimental observation so far, can be realized as collective excitations in a class of condensed matter[10–14] and photonic systems[15–19].

The presence of effective axion fields modifies the equations of electromagnetism which can be presented in the form[12,15,20]

$$\begin{aligned} \mathrm{rot}(-\chi\,\mathbf{E}+\mathbf{H}) &= \frac{1}{c}\frac{\partial}{\partial t}(\mathbf{D}+\chi\,\mathbf{B})+\frac{4\pi}{c}\mathbf{j}, \\ \mathrm{div}(\mathbf{D}+\chi\,\mathbf{B}) &= 4\pi\rho, \end{aligned} \tag{1}$$

$$\mathrm{rot}\,\mathbf{E} = -\frac{1}{c}\frac{\partial \mathbf{B}}{\partial t},\ \mathrm{div}\,\mathbf{B} = 0. \tag{2}$$

Here, ρ and $\mathbf{j}$ are the external charge and current densities, $\mathbf{D} = \varepsilon\,\mathbf{E}$, $\mathbf{B} = \mu\,\mathbf{H}$, while ε and μ are permittivity and permeability of the medium, respectively.

The difference from the conventional electrodynamics appears in the first pair of Maxwell's equations Eqs. (1) and is rooted in the nonzero χ which is called effective axion field in condensed matter literature or Tellegen coefficient in photonics. This term breaks the inversion $\mathcal{P}$ and time-reversal $\mathcal{T}$ symmetries of the system while keeping $\mathcal{PT}$ symmetry preserved.

Interestingly, if χ is time-independent ($\partial\chi/\partial t = 0$) and spatially homogeneous, which is the case for many condensed matter and photonic systems, it does not affect the bulk properties of the medium and arises only at the boundaries. This could be immediately seen from Eqs. (1) by recasting them in the form

$$\begin{aligned} \mathrm{rot}\,\mathbf{H} &= \frac{1}{c}\frac{\partial \mathbf{D}}{\partial t}+\nabla\chi\times\mathbf{E}+\frac{4\pi}{c}\mathbf{j}, \\ \mathrm{div}\,\mathbf{D} &= -\nabla\chi\cdot\mathbf{B}+4\pi\rho. \end{aligned} \tag{3}$$

Hence, χ is a bulk property of the medium, which manifests itself only at the boundary. Partly due to this subtlety, the very existence of Tellegen media was actively disputed in photonics literature[21–24]. By now, the existence of χ response is well established in multiple systems including antiferromagnetic structures, magneto-electrics, multiferroics and three-dimensional topological insulators[12,13]. In the latter case, the axion field plays the role of

School of Physics and Engineering, ITMO University, Saint Petersburg 197101, Russia. e-mail: m.gorlach@metalab.ifmo.ru

a topological invariant and is quantized in units of the fine-structure constant α[6,25] as confirmed experimentally[11].

In turn, nonzero axion response leads to several distinctive physical effects. This includes polarization rotation of light reflected from the axion medium[11], emergence of image magnetic charges induced by the point electric charge above the surface of a topological insulator[26,27], while the field of a point electric dipole surrounded by the axion medium acquires a nonzero magnetic dipole component – the phenomenon known as Witten effect[28–30]. Recently, it was suggested that the axion response can be strongly enhanced in artificial photonic media – metamaterials[15,16] which has been confirmed by the recent experiments[18,19,31] and opened exciting opportunities to experimentally probe various effects of axion electrodynamics.

In condensed matter physics, the axion response is derived through the quantum-mechanical calculation typically utilizing the notion of Berry connection[25] which yields quantized and frequency-independent χ. However, recent studies[32,33] suggest that this picture is simplified and additional effects arise.

In this Article, we approach this field from a different direction and predict the existence of a novel type of electromagnetic response further termed dual axion field, $\tilde{\chi}$. Similarly to the conventional axion, $\tilde{\chi}$ manifests itself only at the boundaries and shares with χ the same parity with respect to the spatial inversion $\mathcal{P}$ and time reversal $\mathcal{T}$. At the same time, the effective theory with $\tilde{\chi}$ leads to the electrodynamics with effective magnetic charge, resulting in the distinct and practically uncharted physics providing a new twist in the effective description of the structured media.

Results

Heuristics of dual axion response

While the theory of axion response in condensed matter systems is well established[6,12,13,25], its origin in classical photonic structures remained much less studied. Electromagnetic community focused on realizing Tellegen particles[16,18,34], while the emergence of the collective Tellegen response was poorly understood.

A useful toy model has recently been provided by ref. 15 which suggested a simple photonic structure based on the stack of layers with gyrotropic permittivity

$$\hat{\varepsilon} = \begin{pmatrix} \varepsilon & ig(z) & 0 \\ -ig(z) & \varepsilon & 0 \\ 0 & 0 & \varepsilon \end{pmatrix}, \tag{4}$$

where out-of-plane magnetization of the layers $g(z)$ is modulated periodically with the zero average [Fig. 1a]. The treatment of this system solely based on Maxwell's equations leads to the axion electrodynamics Eqs. (1), (2) for the averaged fields, where the strength of the effective axion response

$$\chi = -\frac{2\pi a}{\lambda}\int_0^1 g(sa)\, s\, ds \tag{5}$$

is proportional to the period-to-wavelength ratio a/λ and depends on the distribution of magnetization $g(z)$ within the unit cell. Interestingly, χ also depends on the chosen termination of the structure, contrasting with the behavior of the conventional bulk material parameters[35].

Drawing the intuition from this model system, we introduce a similar structure composed of the layers with gyrotropic permeability $\hat{\mu}$

$$\hat{\mu} = \begin{pmatrix} \mu & if(z) & 0 \\ -if(z) & \mu & 0 \\ 0 & 0 & \mu \end{pmatrix}, \tag{6}$$

and a similar periodic distribution of magnetization $f(z)$ [Fig. 1b]. Clearly, such system shares with axion metamaterial the same symmetries with respect to spatial inversion $\mathcal{P}$ and time reversal $\mathcal{T}$. Moreover, given the microscopic (non-averaged) fields **e**, **d**, **b**

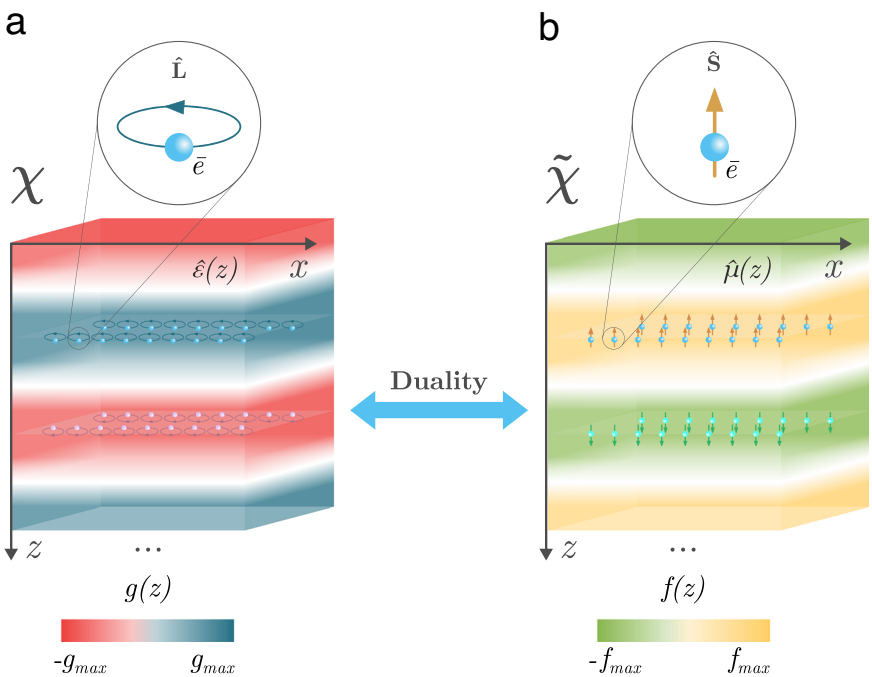

Fig. 1 | Schematic of the two structures with broken $\mathcal{P}$ and $\mathcal{T}$ symmetries but invariant under $\mathcal{PT}$. a Design of the metamaterial with effective axion response χ, ref. 15. Gyrotropic permittivity Eq. (4) is typically associated with the orbital motion, see inset. **b** Metamaterial featuring dual axion response $\tilde{\chi}$. Gyrotropic permeability Eq. (6) is typically due to the spin contribution, see inset.

and **h** in an axion metamaterial, one can immediately find the respective fields in our structure performing the dual symmetry transformation:

$$\begin{aligned}\mathbf{e} &\to \mathbf{h}, \mathbf{d} \to \mathbf{b}, \hat{\varepsilon} \to \hat{\mu} \\ \mathbf{h} &\to -\mathbf{e}, \mathbf{b} \to -\mathbf{d}, \hat{\mu} \to \hat{\varepsilon}.\end{aligned} \tag{7}$$

As a consequence, the effective descriptions of those structures in terms of the averaged fields should also be related to each other via the same duality transformation, Eq. (7). This yields the set of electrodynamics equations

$$\mathrm{rot}\,\mathbf{H} = \frac{1}{c}\frac{\partial \mathbf{D}}{\partial t} + \frac{4\pi}{c}\mathbf{j}, \mathrm{div}\,\mathbf{D} = 4\pi\rho, \tag{8}$$

$$\begin{aligned}\mathrm{rot}(\mathbf{E} + \tilde{\chi}\,\mathbf{H}) &= -\frac{1}{c}\frac{\partial}{\partial t}(\mathbf{B} - \tilde{\chi}\,\mathbf{D}), \\ \mathrm{div}(\mathbf{B} - \tilde{\chi}\,\mathbf{D}) &= 0,\end{aligned} \tag{9}$$

where $\mathbf{D} = \varepsilon\,\mathbf{E}$, $\mathbf{B} = \mu\,\mathbf{H}$ and dual axion field reads

$$\tilde{\chi} = -\frac{2\pi a}{\lambda}\int_0^1 f(sa)\,s\,ds, \tag{10}$$

while the distribution of external sources ρ and $\mathbf{j}$ is defined by the experimental conditions. For consistency, we provide an independent and complete derivation of Eqs. (8)–(10) in the Supplementary Notes 1 and 2.

Crucially, the corrections appear now in the second pair of Maxwell's equations Eqs. (9) which are normally used to define the potentials. This distinguishes our model from the effective theories studied previously and opens further opportunities. For instance, χ and $\tilde{\chi}$ responses may coexist in metamaterials combining both gyrotropic permittivity and permeability modulated in space, see Supplementary Note 3.

In analogy to the axion field, $\tilde{\chi}$ reduces to the boundary term provided $\partial\tilde{\chi}/\partial t = 0$. Below, we explore the consequences of electrodynamics Eqs. (8), (9) and suggest experimentally observable distinctions of the axion field χ from its dual, $\tilde{\chi}$. In addition, we provide a Lagrangian formulation of this theory (Supplementary Note 4) using a two-potential framework.

Effective magnetic charges and optical properties

Evidently, Eqs. (8)–(9) describe the effective theory with magnetic charge[36] when Maxwell's equations take the form

$$\mathrm{rot}\,\mathbf{H} = \frac{1}{c}\frac{\partial \mathbf{D}}{\partial t} + \frac{4\pi}{c}\mathbf{j}, \mathrm{div}\,\mathbf{D} = 4\pi\rho, \tag{11}$$

$$\mathrm{rot}\,\mathbf{E} = -\frac{1}{c}\frac{\partial \mathbf{B}}{\partial t} - \frac{4\pi}{c}\mathbf{j}_m, \mathrm{div}\,\mathbf{B} = 4\pi\rho_m, \tag{12}$$

where ρ_m and $\mathbf{j}_m$ describe the density of magnetic charges and currents. In our case, those quantities are

$$\rho_m = \frac{1}{4\pi}\mathrm{div}(\tilde{\chi}\,\mathbf{D}), \tag{13}$$

$$\mathbf{j}_m = -\frac{1}{4\pi}\frac{\partial}{\partial t}(\tilde{\chi}\,\mathbf{D}) + \frac{c}{4\pi}\mathrm{rot}(\tilde{\chi}\,\mathbf{H}), \tag{14}$$

satisfying the usual continuity equation $\partial\rho_m/\partial t + \mathrm{div}\,\mathbf{j}_m = 0$.

The total magnetic charge of a finite volume of the medium with $\tilde{\chi}$ response can be readily computed as

$$g \equiv \int \rho_m\,dV = \frac{1}{4\pi}\oint \tilde{\chi}\,\mathbf{D}\cdot\mathbf{n}\,df = 0 \tag{15}$$

as $\tilde{\chi}$ vanishes outside of the medium. Therefore, the introduced effective description does not yield any uncompensated magnetic charges.

Next we examine the phenomena at the boundary of a homogeneous $\tilde{\chi}$ medium. To that end, we integrate Eqs. (8), (9) over a pillbox. Assuming no external surface charges or currents, we obtain the set of boundary conditions

$$\mathbf{H}_{1t} = \mathbf{H}_{2t}, D_{1n} = D_{2n}, \tag{16}$$

$$\mathbf{E}_{1t} + \tilde{\chi}_1\,\mathbf{H}_{1t} = \mathbf{E}_{2t} + \tilde{\chi}_2\,\mathbf{H}_{2t}, \tag{17}$$

$$B_{1n} - \tilde{\chi}_1 D_{1n} = B_{2n} - \tilde{\chi}_2 D_{2n}. \tag{18}$$

The tangential components of **E** and normal component of **B** now experience the discontinuity, which is not typical for the conventional media, but becomes possible here since we consider the averaged fields.

To illustrate the physics behind the boundary conditions Eqs. (16)–(18), we examine a homogeneous slab of $\tilde{\chi}$ medium with the thickness L in vacuum calculating reflection and transmission coefficients for the linearly polarized plane wave at normal incidence as

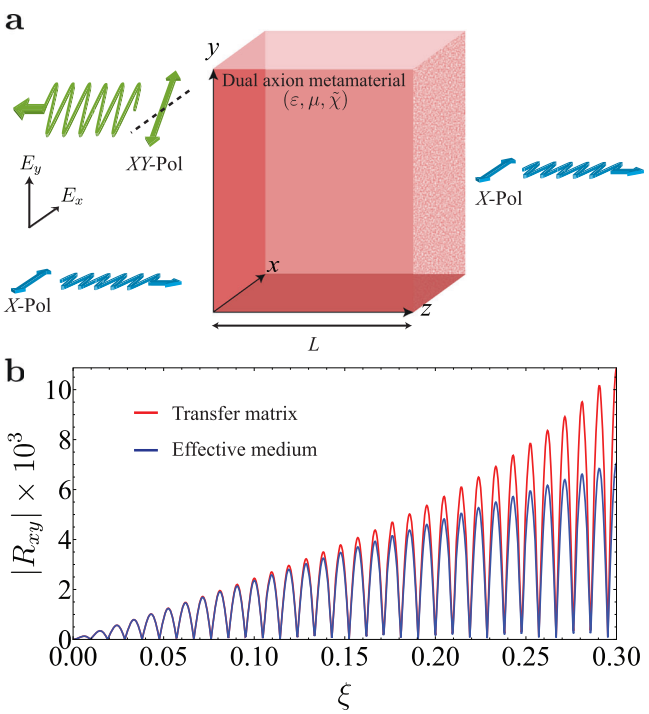

Fig. 2 | Probing the response of the dual axion medium to the incident plane waves. a Transmitted and reflected waves in a dual axion slab excited by the incident x-polarized plane wave. The polarization of reflected wave is rotated due to the Kerr effect, Eq. (19). **b** Cross-polarized reflection coefficient for the metamaterial slab consisting of $N = 50$ periods calculated via transfer matrix method (red) and effective medium approach (blue) versus $\xi = a/\lambda$. Parameters of the gyrotropic layers in the transfer matrix simulation are $\varepsilon = 1.05$, $\mu = 1.05$, $f_0 = 0.015$. For effective medium description, we choose $\varepsilon_{\mathrm{eff}} = 1.05$, $\mu_{\mathrm{eff}} = \mu + \frac{\pi^2}{12}|f_0|^2\xi^2$, $\tilde{\chi}_{\mathrm{eff}} = \frac{\pi}{2}f_0\,\xi$ and $kL = 2\pi\sqrt{\varepsilon_{\mathrm{eff}}\mu_{\mathrm{eff}}}Na/\lambda$.

shown in Fig. 2a. In close analogy to the conventional axion media, the polarization plane of reflected light is rotated as captured by the cross-polarized reflection coefficient R_{xy}, while cross-polarized transmission T_{xy} vanishes (see Supplementary Note 5):

$$R_{xy} = -R_{yx} = -2\tilde{\chi}\,\sin(kL)/\Delta, \tag{19}$$

$$T_{xy} = T_{yx} = 0, \tag{20}$$

where k is the propagation constant inside the slab,

$$\Delta = 2iZ\,\cos kL + \left(1 + Z^2 + \tilde{\chi}^2\right)\,\sin kL \tag{21}$$

and $Z = \sqrt{\mu/\varepsilon}$ is the impedance. To check the accuracy of the above predictions of $\tilde{\chi}$ electrodynamics, we simulate the metamaterial composed of pairs of oppositely magnetized gyrotropic layers with the period a using the rigorous transfer matrix method. In Fig. 2b we compare the two approaches by fixing the thickness of a metamaterial slab and varying the wavelength of the incident light such that a/λ ratio spans the range from 0 to 0.3. We observe that the effective description of metamaterial in terms of $\tilde{\chi}$ is consistent provided the period of the structure a is at least an order of magnitude smaller than the wavelength of light λ: $\xi = a/\lambda < 0.15$. The same applies to all remaining co- and cross-polarized reflection and transmission coefficients as further analyzed in Supplementary Note 6 and Supplementary Fig. 2.

Similarity and distinction of χ and $\tilde{\chi}$ responses

Vanishing cross-polarized transmission and nonzero cross-polarized reflection is typically considered as a smoking gun for the effective axion response[16,18,37], which can be distinguished in this way from the magneto-optical phenomena (gyrotropy) or electromagnetic chirality. The results above suggest that $\tilde{\chi}$ response behaves exactly in the same way.

Quite remarkably, the parallel between χ and $\tilde{\chi}$ responses extends much further. As we prove in the Supplementary Note 7, if the electromagnetic fields are measured outside of the metamaterial, and the sources are positioned outside as well, the behavior of $\tilde{\chi}$ medium with permittivity ε and permeability μ is indistinguishable from the axion medium with the following effective material parameters:

$$\varepsilon_{\text{eff}} = \frac{\varepsilon\mu}{\mu + \varepsilon\tilde{\chi}^2}, \tag{22}$$

$$\mu_{\text{eff}} = \mu + \varepsilon\tilde{\chi}^2, \tag{23}$$

$$\chi_{\text{eff}} = -\frac{\varepsilon\tilde{\chi}}{\mu + \varepsilon\tilde{\chi}^2}. \tag{24}$$

As elaborated in the Supplementary Note 7, the mapping Eqs. (22)–(24) builds on the possibility to redefine the averaged fields **E** and **B** inside the metamaterial without any modification of the fields outside.

Based on this mapping, we conclude that χ and $\tilde{\chi}$ responses cannot be distinguished in any sort of the scattering experiment typically used to capture the effective axion response.

However, despite the remarkable parallel between χ and $\tilde{\chi}$ fields, they are manifested differently when the external sources are introduced into the medium. Experimentally relevant examples of such situations in condensed matter include bremsstrahlung, Cherenkov and transition radiation or ionization losses of charged particles moving through the material. In photonics context, one could introduce an antenna directly inside the metamaterial. Here, for conceptual clarity, we focus on the situation when the metamaterial sphere is excited by the external electric dipole antenna as depicted in Fig. 3a, d.

Theoretical analysis of this problem suggests that the field outside of the sphere is a superposition of electric and magnetic dipole fields (see Supplementary Note 8 and Supplementary Fig. 4). Such mixing of

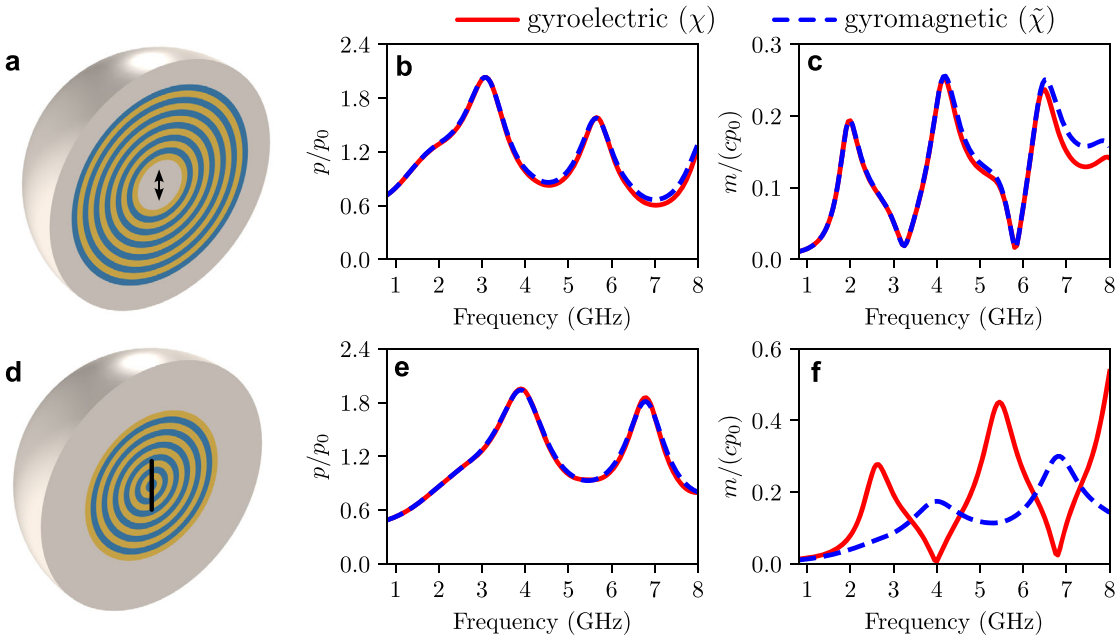

Fig. 3 | Distinguishing axion χ and dual axion $\tilde{\chi}$ responses of the medium via the coupling to the external sources in a spherical geometry. a Point electric dipole inside an air cavity within a spherical metamaterial consisting of radially magnetized layers with alternating magnetization direction. The layers possess either gyrotropic permittivity, i.e., $\mathbf{D} = \varepsilon\mathbf{E} \pm ig_e\mathbf{E}\times\hat{\mathbf{r}}$ (χ case) or gyrotropic permeability, i.e., $\mathbf{B} = \mu\mathbf{H} \pm ig_m\mathbf{H}\times\hat{\mathbf{r}}$ ($\tilde{\chi}$ case). The thickness of each layer is $t = 2$ mm, the cavity radius is $3t$; the material parameters $\varepsilon = 5$, $g_e = 4$, $\mu = 1$, $g_m = -0.8$ ensure the mapping (25). **d** A linear antenna of length $4t$ inside the metamaterial. The core layer has zero magnetization. **b**, **c**, **e**, **f** Effective electric and magnetic dipole moments of the system retrieved from the far field calculated for geometries (**a**, **d**), respectively. The results are normalized to the dipole moment of antenna in the absence of metamaterial. Solid red and dashed blue curves correspond to χ and $\tilde{\chi}$ responses, respectively.

electric and magnetic multipoles occurs due to the simultaneous breaking of $\mathcal{P}$ and $\mathcal{T}$ symmetries by the medium and hence should take place both for χ and $\tilde{\chi}$ metamaterials. However, the quantitative details for χ and $\tilde{\chi}$ media are different (see Supplementary Note 9).

First, we simulate the excitation of a metamaterial sphere with a spherical void, Fig. 3a. If the sphere is composed of layers with gyrotropic permittivity, specifically, $\mathbf{D}=\varepsilon\mathbf{E}\pm ig_e\mathbf{E}\times\hat{\mathbf{r}}$, it features the conventional axion response χ. The retrieved dipole moments for the different excitation frequencies are shown by the red lines in Fig. 3b, c. On the other hand, if the layers possess gyrotropic permeability, i.e., $\mathbf{B}=\mu\mathbf{H}\pm ig_m\mathbf{H}\times\hat{\mathbf{r}}$, the metamaterial sphere exhibits $\tilde{\chi}$ response. The calculated effective dipole moments in such case are shown by the dashed blue lines in Fig. 3b, c. To compare the two scenarios, we choose the same permittivity ε and permeability μ for both simulations, while electric and magnetic gyrotropy are linked to each other as

$$g_m=-\frac{\mu}{\varepsilon}g_e, \tag{25}$$

which guarantees that the effective responses χ and $\tilde{\chi}$ satisfy the mapping Eqs. (22)–(24) up to the second-order corrections in χ or $\tilde{\chi}$.

Comparing the retrieved dipole moments [Fig. 3b, c], we observe that the results for χ and $\tilde{\chi}$ scenarios coincide. Since the dipole is located in an air void outside of the metamaterial, this fully agrees with our theoretical analysis and provides a numerical confirmation of the mapping Eqs. (22)–(24), while small discrepancy between the two scenarios in the high-frequency region should be attributed to the limitations of the effective medium description.

Second, we analyze more interesting scenario when the external sources are introduced directly inside the metamaterial, Fig. 3d. In such case, the distinction between χ and $\tilde{\chi}$ spheres arises already in electrostatic limit (see Supplementary Note 8). Specifically, χ and $\tilde{\chi}$ spheres excited by the point electric dipole $\mathbf{d}_0$ develop the effective dipole moments

$$\mathbf{d}_\chi\approx\frac{3}{\varepsilon+2}\mathbf{d}_0,\mathbf{m}_\chi\approx-\frac{3\mu\chi}{(\varepsilon+2)(\mu+2)}\mathbf{d}_0, \tag{26}$$

$$\mathbf{d}_{\tilde{\chi}}\approx\frac{3}{\varepsilon+2}\mathbf{d}_0,\mathbf{m}_{\tilde{\chi}}\approx-\frac{6\tilde{\chi}}{(\varepsilon+2)(\mu+2)}\mathbf{d}_0, \tag{27}$$

where the terms proportional to χ^2 or $\tilde{\chi}^2$ are omitted for clarity. Thus, the effective electric dipole moments coincide, while the induced magnetic dipoles differ and are not connected to each other by the mapping Eqs. (22)–(24).

To confirm that intuition, we simulate the excitation of χ and $\tilde{\chi}$ metamaterials in the same frequency range $f=(1\div8)$ GHz in the absence of voids. In this case, χ and $\tilde{\chi}$ span the ranges $(0.08\div0.67)$ and $(0.02\div0.13)$, respectively. This time an electric dipole antenna has a finite size [Fig. 3d] such that spatial dispersion effects are suppressed and effective medium treatment remains adequate.

In agreement with our analytical solution (see Supplementary Note 9 and Supplementary Fig. 5), the induced electric dipole moments of both spheres coincide which confirms that the effective medium treatment is valid in this geometry as well [Fig. 3e]. However, the induced magnetic dipole moments of χ and $\tilde{\chi}$ spheres are profoundly distinct featuring completely different frequency dependence [Fig. 3f] which thus distinguishes χ and $\tilde{\chi}$ physics.

The origin of such distinction can be traced back to the mapping Eqs. (22)–(24): $\tilde{\chi}$ medium with the external electric sources maps onto the usual axion medium χ excited by the combination of electric and magnetic sources (see Supplementary Note 9). Notably, such distinction exists even in the presence of moderate losses, even though the resonant peaks become less visible (see Supplementary Note 10 and Supplementary Fig. 6).

An interesting further question is the transition between the situations depicted in Fig. 3a, d. To probe that, we fix the size of the cavity in the metamaterial simulating its excitation by the antennas of the different size (see Supplementary Note 10 and Supplementary Fig. 7). In short, if the antenna size is smaller than the size of the cavity, the results for χ and $\tilde{\chi}$ media closely match highlighting the validity of the mapping Eqs. (22)–(24). However, once the antenna size exceeds the diameter of the cavity and antenna penetrates in the bulk of the metamaterial, the distinctions start to show up (see Supplementary Fig. 7). These results once again highlight a subtle nature of the difference between axion and dual axion media.

Importantly, the existence of the dual axion field results not only in the quantitative corrections to the axion electrodynamics, but also in the qualitatively new phenomena. To illustrate that, we consider a spherical meta-structure featuring the combination of axion and dual axion responses such that $\chi=\varepsilon\tilde{\chi}/\mu$. This ratio between the two nonreciprocal responses ensures that the arbitrary excitation of such a setup by the incident wave does not reveal any kind of non-reciprocity. The meta-structure scatters as a usual dielectric particle with well-defined permittivity and permeability (see Supplementary Note 11).

However, if the setup is excited by the point electric dipole placed inside it, the radiated far field contains both electric and magnetic dipole contributions. Hence, this system features an intrinsic non-reciprocity which can not be retrieved in any scattering experiment, but manifests itself when excited by the introduced external sources.

Suggested experiments

While the spherical setup Fig. 3a, d provides a transparent physical picture, the actual axion or dual axion materials in condensed matter and photonics have a planar geometry [Fig. 4a, d]. Below, we suggest the potential experimental scheme allowing to distinguish and measure χ and $\tilde{\chi}$ for non-reciprocal magneto-electric metamaterials[16,18]. As a specific example, we consider a stack of 18 gyrotropic layers. Each unit cell consists of a pair of oppositely magnetized layers, each with the thickness $t=2$ mm, i.e., 9 unit cells in total [Fig. 4a].

First, we examine the reflection and transmission of a plane wave incident at the metamaterial slab with either χ or $\tilde{\chi}$ response [Fig. 4a]. Since the parameters of the two structures are related via the mapping, Eqs. (22)–(24), the results for reflection and transmission coincide in the entire studied frequency range including both co- and cross-polarized scattering [Fig. 4b, c].

To distinguish between the two responses, we consider the excitation of the same metamaterials by the external source introduced in the middle of the slab. In our simulations [Fig. 4d], this is an infinite wire parallel to the layers and carrying an alternating current. To minimize the role of the side surfaces, we apply the periodic boundary conditions in the transverse direction, which physically corresponds to the excitation of an infinite metamaterial by the periodic array of in-phase wires. Next we evaluate the radiated electric field outside of the structure extracting the components of the field parallel and orthogonal to the wire axis, further denoted as co- and cross-polarized components, at the distance 1.25λ from the upper boundary of the structure. These fields are further normalized to the characteristic field $\mu_0 I_0\omega/4$ produced by the single wire with AC current in vacuum at the distance $r=0.0872\lambda$ from the center of the wire. We observe that the co-polarized fields for χ and $\tilde{\chi}$ scenarios match quite closely [Fig. 4e], while the cross-polarized components are markedly different [Fig. 4f] capturing the distinct physics of axion and dual axion media. We expect that such a distinction can be observed in the recently realized microwave Tellegen metamaterials[18] which feature strong axion-type response.

Qualitatively similar results are obtained when the multilayered structure is excited by the point electric dipole parallel to the layers (see Supplementary Fig. 8). Thus, the difference between χ and $\tilde{\chi}$ responses is quite robust and can be probed experimentally exciting the structure by the different types of sources.

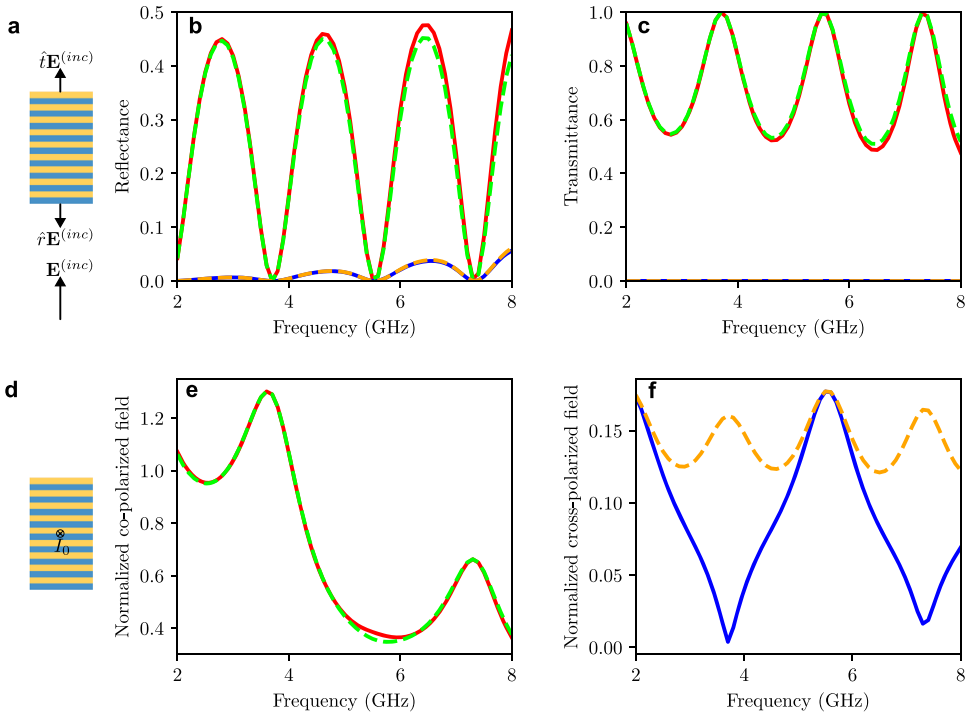

Fig. 4 | Exploring the distinction between axion and dual axion response in a planar geometry. a Scheme of a plane wave excitation of a multilayered slab. Different colors encode different magnetization of the layers. Overall there are 18 layers, i.e., 9 unit cells. The period of the lattice $a = 4$ mm, parameters of the axion metamaterial are $\varepsilon = 5$, $\mu = 1$, $g_e = 4$, so $\chi = (\pi/2) g_e (a/\lambda)$. Parameters of the dual axion medium are found from the mapping (22)–(24), $g_m = (2/\pi)\tilde{\chi}(\lambda/a)$. **b**, **c** The reflectance and transmittance spectra, $|R|^2$ and $|T|^2$. Solid and dashed lines correspond to the axion and dual axion case, respectively. Red and green lines correspond to the co-polarized scattering, blue and orange lines depict the cross-polarized scattering. **d** Scheme of the excitation by the line current parallel to the layers. The parameters are the same as in panel (**a**). In the transverse direction, the structure is periodic with the period $5a = 20$ mm. **e**, **f** Far fields above the multilayered slab normalized to the characteristic field $\mu_0 I_0 \omega/4$ produced by the single wire.

Discussion

These results bring us to the conclusion that there exists a distinct type of $\mathcal{P}$- and $\mathcal{T}$-odd electromagnetic response which, to the best of our knowledge, has not been identified previously. Similarly to the effective axion field, it is not manifested in the bulk of a stationary medium, but has profound boundary signatures captured by the effective theory Eqs. (8), (9) with the boundary conditions Eqs. (16)–(18). The predicted response $\tilde{\chi}$ is a distinct physical entity as it can be distinguished from the conventional axion field in experiments.

Here, we have put forward a single example of metamaterial realizing this physics on a photonic platform. Using the same line of thought, it is also possible to design metamaterials featuring χ and $\tilde{\chi}$ responses simultaneously (see Supplementary Note 3). We anticipate that the predicted response is general and arises in many condensed matter systems, where it could have been misidentified as an effective axion field. Nonzero χ and $\tilde{\chi}$ may coexist or continuously transform one into another with the change of the field frequency, lattice geometry or other parameters.

Based on our analysis, we hypothesize that χ and $\tilde{\chi}$ fields are related to the orbital and spin contributions to the magnetization. However, quantum-mechanical theory of $\tilde{\chi}$ response in condensed matter remains an interesting open problem. Another open question is the possibility of $\tilde{\chi}$ field quantized by the symmetries of the structure.

Methods

Effective medium description of dual axion response

We performed numerical validation of the effective medium description by comparing the transmission and reflection coefficients calculated via the transfer matrix method with those obtained from the effective theoretical model. This analysis was conducted for both axion and dual axion metamaterials. The agreement between the two approaches verifies the accuracy of the effective medium description in the subwavelength regime.

Simulations

Full-wave numerical simulations were conducted using COMSOL Multiphysics to generate the results shown in Figs. 3 and 4 in the main text, as well as Supplementary Figs. 6–8. Periodic boundary conditions were applied in the transverse directions to minimize finite-size effects for the simulated metamaterial slabs. This approach was used to model both the 2D and 3D experimental configurations for distinguishing χ and $\tilde{\chi}$ responses.

Data availability

The data that support the findings of this study are available from the corresponding author upon request.

References

1. Bernevig, B. A., Hughes, T. L. & Zhang, S.-C. Quantum Spin Hall Effect and topological phase transition in HgTe quantum wells. *Science* **314**, 1757 (2006).
2. Raghu, S. & Haldane, F. D. M. Analogs of quantum-Hall-effect edge states in photonic crystals. *Phys. Rev. A* **78**, 033834 (2008).
3. Shen, S.-Q. et al. *Topological Insulators. Dirac Equation in Condensed Matters*. (Springer, Heidelberg, 2012).
4. Tong, D. et al. Lectures on the quantum Hall effect. Preprint at *arXiv* https://doi.org/10.48550/ARXIV.1606.06687 (2016).
5. Greiter, M. & Wilczek, F. Fractional statistics. *Annu. Rev. Condens. Matter Phys.* **15**, 131–157 (2024).
6. Qi, X.-L., Hughes, T. L. & Zhang, S.-C. Topological field theory of time-reversal invariant insulators. *Phys. Rev. B* **78**, 195424 (2008).

7. You, Y., Burnell, F. J. & Hughes, T. L. Multipolar topological field theories: Bridging higher order topological insulators and fractons. *Phys. Rev. B* **103**, 245128 (2021).
8. Wilczek, F. Problem of Strong P and T Invariance in the Presence of Instantons. *Phys. Rev. Lett.* **40**, 279 (1978).
9. Weinberg, S. A New Light Boson? *Phys. Rev. Lett.* **40**, 223 (1978).
10. Li, R., Wang, J., Qi, X.-L. & Zhang, S.-C. Dynamical axion field in topological magnetic insulators. *Nat. Phys.* **6**, 284 (2010).
11. Wu, L. et al. Quantized Faraday and Kerr rotation and axion electrodynamics of a 3D topological insulator. *Science* **354**, 1124 (2016).
12. Nenno, D. M., Garcia, C. A. C., Gooth, J., Felser, C. & Narang, P. Axion physics in condensed-matter systems. *Nat. Rev. Phys.* **2**, 682 (2020).
13. Sekine, A. & Nomura, K. Axion electrodynamics in topological materials. *J. Appl. Phys.* **129**, 141101 (2021).
14. Qiu, J.-X. et al. Observation of the axion quasiparticle in 2D MnBi2Te4. *Nature* **641**, 62–69 (2025).
15. Shaposhnikov, L., Mazanov, M., Bobylev, D. A., Wilczek, F. & Gorlach, M. A. Emergent axion response in multilayered metamaterials. *Phys. Rev. B* **108**, 115101 (2023).
16. Safaei Jazi, S. et al. Optical Tellegen metamaterial with spontaneous magnetization. *Nat. Commun.* **15**, 1293 (2024).
17. Devescovi, C. et al. Axion topology in photonic crystal domain walls. *Nat. Commun.* **15**, 6814 (2024).
18. Yang, Q., Wen, X., Li, Z., You, O. & Zhang, S. Gigantic Tellegen responses in metamaterials. *Nat. Commun.* **16**, 151 (2025).
19. Jazi, S. S.et al. Realization of the Tellegen effect in resonant optical metasurfaces, Preprint at *arXiv* https://doi.org/10.48550/ARXIV.2503.22184 (2025).
20. Wilczek, F. Two applications of axion electrodynamics. *Phys. Rev. Lett.* **58**, 1799 (1987).
21. Post, E. J. & Seeger, R. J. Formal structure of electromagnetics. *Am. J. Phys.* **33**, 597 (1965).
22. Lakhtakia, A. & Weiglhofer, W. Are linear, nonreciprocal, biisotropic media forbidden? *IEEE Trans. Microw. Theory Tech.* **42**, 1715 (1994)
23. Sihvola, A. Are nonreciprocal bi-isotropic media forbidden indeed? *IEEE Trans. Microw. Theory Tech.* **43**, 2160 (1995).
24. Serdyukov, A., Semchenko, I., Tretyakov, S. & Sihvola, A. *Electromagnetics of Bi-anisotropic Materials: Theory and Applications*. (Gordon and Breach Science Publishers, Amsterdam, 2001).
25. Essin, A. M., Moore, J. E. & Vanderbilt, D. Magnetoelectric polarizability and axion electrodynamics in crystalline insulators. *Phys. Rev. Lett.* **102**, 146805 (2009).
26. Qi, X.-L., Li, R., Zang, J. & Zhang, S.-C. Inducing a magnetic monopole with topological surface states. *Science* **323**, 1184 (2009).
27. Uri, A. et al. Nanoscale imaging of equilibrium quantum Hall edge currents and of the magnetic monopole response in graphene. *Nat. Phys.* **16**, 164 (2019).
28. Witten, E. Dyons of charge $e\theta/2\pi$. *Phys. Lett. B* **86**, 283 (1979).
29. Rosenberg, G. & Franz, M. Witten effect in a crystalline topological insulator. *Phys. Rev. B* **82**, 035105 (2010).
30. Seidov, T. Z. & Gorlach, M. A. Hybridization of electric and magnetic responses in the effective axion background. *Phys. Rev. A* **108**, 053515 (2023).
31. Liu, G.-G. et al. Photonic axion insulator. *Science* **387**, 162 (2025).
32. Ahn, J., Xu, S.-Y. & Vishwanath, A. Theory of optical axion electrodynamics and application to the Kerr effect in topological antiferromagnets. *Nat. Commun.* **13**, 7615 (2022).
33. Wang, M., Liu, H. & Xie, X. New type of anticommutative dynamical magnetoelectric response. *Phys. Rev. Lett.* **128**, 236601 (2022).
34. Tretyakov, S. A. et al. Artificial Tellegen Particle. *Electromagnetics* **23**, 665 (2003).
35. Alù, A. First-principles homogenization theory for periodic metamaterials. *Phys. Rev. B* **84**, 075153 (2011).
36. Shnir, Y. *Magnetic Monopoles*. (Springer-Verlag, Berlin, 2005).
37. Qiu, J.-X. et al. Axion optical induction of antiferromagnetic order. *Nat. Mater.* **22**, 583 (2023).

Acknowledgements

We acknowledge Alexey Gorlach for valuable discussions. Theoretical models were supported by the Russian Science Foundation (grant No. 23-72-10026), numerical simulations were supported by Priority 2030 Federal Academic Leadership Program. The authors acknowledge partial support by the Foundation for the Advancement of Theoretical Physics and Mathematics "Basis".

Author contributions

M.A.G. conceived the idea and supervised the project. T.Z.S. derived the Lagrangian description, together with M.A.G. developed the analytical model for the dipole excitation, together with E.B.-A. elaborated the mapping between χ and $\tilde{\chi}$ responses. E.B.-A. also analyzed the scattering from the metamaterial slab and performed transfer matrix calculations. D.A.B. performed full-wave numerical simulations of the dipole excitation. L.S., together with M.A.G., derived an effective description of $\tilde{\chi}$ metamaterial. M.M. contributed to the transfer matrix simulation of χ and $\tilde{\chi}$ media. D.A.B. and E.B.-A. elaborated the proposal for experimental observation of $\tilde{\chi}$. All authors contributed to the manuscript preparation.

Competing interests

The authors declare no competing interests.

Additional information

Supplementary information The online version contains supplementary material available at https://doi.org/10.1038/s41467-025-61183-5.

Correspondence and requests for materials should be addressed to Maxim A. Gorlach.

Peer review information *Nature Communications* thanks Francesca Chadha-Day and the other, anonymous, reviewer(s) for their contribution to the peer review of this work. A peer review file is available.